Dalton Transactions

Dynamic Article Links

Cite this: *Dalton Trans.*, 2012, **41**, 5055

www.rsc.org/dalton

PAPER

Preparation and electrochemistry of Pd–Ni/Si nanowire nanocomposite catalytic anode for direct ethanol fuel cell

Fengjuan Miao,[a,b] Bairui Tao*[a,b] and Paul K. Chu[c]

Received 24th December 2011, Accepted 7th February 2012
DOI: 10.1039/c2dt12486f

A new silicon-based anode suitable for direct ethanol fuel cells (DEFCs) is described. Pd–Ni nanoparticles are coated on Si nanowires (SiNWs) by electroless co-plating to form the catalytic materials. The electrocatalytic properties of the SiNWs and ethanol oxidation on the Pd–Ni catalyst (Pd–Ni/SiNWs) are investigated electrochemically. The effects of temperature and working potential limit in the anodic direction on ethanol oxidation are studied by cyclic voltammetry. The Pd–Ni/SiNWs electrode exhibits higher electrocatalytic activity and better long-term stability in an alkaline solution. It also yields a larger current density and negative onset potential thus boding well for its application to fuel cells.

1. Introduction

Electrooxidation of alcohols such as methanol, ethanol, propanol, and butanol has attracted much attention due to the rapid development of direct alcohol fuel cells (DAFCs).[1] In particular, direct ethanol fuel cells (DEFCs) are recognized as a promising clean energy source for portable electronic devices and transportation because ethanol is non-toxic and has a high energy density (~8 kW h kg^{-1}).[2] In addition, it can be readily produced in large quantities by fermentation of sugar-containing raw materials.[3–6] The electrocatalyst is one of the key components in a DEFC and Pt has been extensively investigated as the electrocatalyst for ethanol oxidation.[7] However, electrooxidation of ethanol on Pt may produce CO which can rapidly deteriorate the catalytic performance, and binary catalysts such as Pt–Ru and Pt–Sn have been proposed to mitigate CO poisoning.[8–10] Nonetheless, the high price and limited supply of Pt constitute the major barriers for commercial development of this type of DEFCs and it is important to develop low-cost non-platinum electrocatalysts with suitable kinetics.

Pd is a good electrocatalyst for ethanol oxidation in an alkaline medium due to the high current density and good stability.[11] Other common metals such as Co,[12] Ni,[13] and Fe[14] have also been proposed to be electrocatalysts for organic synthesis in an alkaline medium[15] and for instance, Ni alloying can improve methanol oxidation.[16] Current research efforts focus on the development of anode electrocatalysts with high utilization efficiency. Usually, these electrocatalysts are dispersed on a conducting substrate with a large surface area such as carbonized TiO_2 or SnO_2 nanotubes,[17,18] hollow carbon nanotubes,[19] MnO_2 nanotubes,[20] and so on. Xu *et al.* [21] reported that Pd–C had a higher catalytic activity and better steady-state ethanol oxidation characteristics than Pt–C, and Pd–C could promote oxides such as CeO_2 and NiO. The catalytic activity was higher than that of commercial E-TEK PtPu–C for the same noble metal loading.[22] Ryoo *et al.* [23–25] reported that by using 3D ordered mesoporous carbon (OMC) as the support for metal nanocatalysts, excellent electrooxidation performance could be achieved. Considering the cost and size in large-scale fabrication, the on-chip integration compatibility with other electronic components is necessary. Therefore, monolithic integration of Si-based microfabricated fuel cells is important. In this work, palladium-nickel nanoparticles are prepared on silicon nanowires (SiNWs) by electroless co-plating and the electrochemical properties of the resulting Pd–Ni/SiNWs are investigated.

2. Experimental details

All reagent grade chemicals were analytical grade and used without further purification. The SiNWs were synthesized using procedures described previously.[26] In brief, N-type ⟨100⟩ silicon wafers with a resistivity of 0.006–0.02 Ω cm were cleaned with acetone, ethanol, deionized water, and a buffered oxide etching solution. The cleaned silicon wafers were immersed in an aqueous HF solution containing silver nitrate for 40 min at room temperature. After etching, the silicon wafers were rinsed with diluted HNO_3 to detach the loose silver from the SiNWs surface and the silicon wafers were then rinsed with deionized water and dried at 30 °C by nitrogen.

The Pd–Ni/SiNWs structure was fabricated using the following procedure. The SiNWs were cut into rectangular pieces, cleaned with deionized water, and activated in Triton X-100 for 60 sec, and the Pd–Ni/SiNWs nanocomposites were prepared by fully coating with nickel and plating a thin Pd shell on the Ni/

[a]*College of Communications and Electronics Engineering, Qiqihar University, 42 Wenhua Street, Qiqihar, Heilongjiang 161006, China*
[b]*National Laboratory for Infrared Physics, Shanghai Institute of Technical Physics, Chinese Academy of Sciences, Shanghai 200083, China. E-mail: tbr_sir@163.com; Fax: +(86-452) 2738748; Tel: +(86-452) 2742787*
[c]*Department of Physics and Material Sciences, City University of Hong Kong, Tat Chee Avenue, Kowloon, Hong Kong, China*

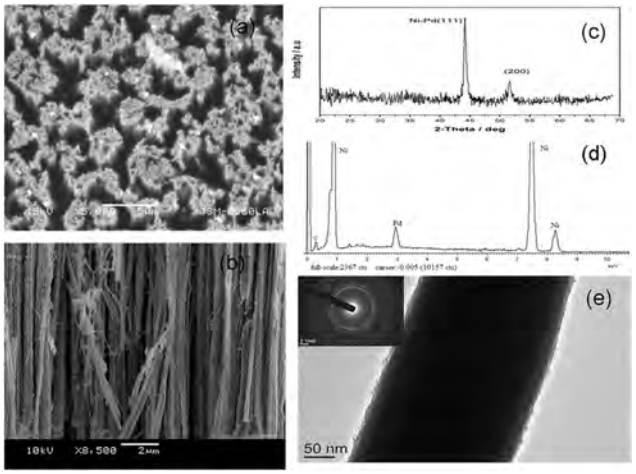

Fig. 1 (a): Top-view SEM images of the microstructure of the Pd–Ni/SiNWs, (b): cross-sectional SEM images of the microstructure of the Pd–Ni/SiNWs, (c): XRD image of the structure in Fig. 1(b), (d): corresponding EDS image of the structure in Fig. 1(b), and (e): TEM image of the microstructure together with selected area electron diffraction (SAED) patterns of the Pd–Ni/SiNWs (inset in Fig. 1(e)).

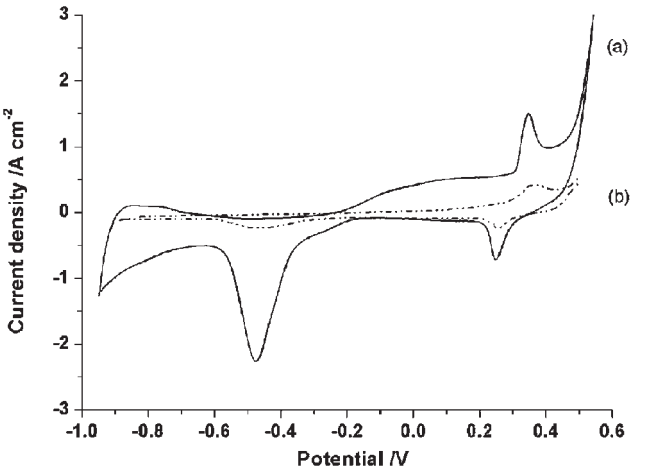

Fig. 2 Cyclic voltammograms of (a) Pd–Ni/SiNWs and (b) Pd–Ni/Si acquired in 1 M KOH solution at room temperature at a scanning rate of 50 mV s^{-1}.

SiNWs core. The samples were coated with Ni and trace Pd simultaneously for 25 min by electroless co-plating: for the electroless Ni–Pd plating, $PdCl_2$ (20 mg L^{-1}) is added into the bath of electroless plating nickel. During deposition, the temperature was kept at 86 °C with continuous stirring. The pH value was adjusted by addition of ammonia.[27] Afterwards, the Pd–Ni/SiNWs nanocomposites were rapidly thermally annealed at 400 °C for 60 s under Ar to produce nickel silicide which offered better resistance in alkaline media.[28] A copper wire was glued to the Pd–Ni/SiNWs chips.

The morphology and composition of the Pd–Ni/SiNWs electrodes were characterized by scanning electron microscopy (SEM), transmission electron microscopy (TEM), and energy-dispersive X-ray spectroscopy (EDS). Electrochemical measurements were carried out on a tri-electrode system consisting of a platinum foil counter electrode, saturated Ag–AgCl reference electrode, and Pd–Ni/SiNWs working electrode. The experiments were conducted at 25 °C and under 1 atmospheric pressure.

3. Results and discussion

Fig. 1(a) and 1(b) display the representative top-view and cross-sectional SEM images of the Pd–Ni/SiNWs and Fig. 1(c) and 1(d) depict the XRD and EDS image of the structure in Fig. 1 (e), respectively. The Pd–Ni/SiNWs have a bundled morphology with a nanowire length of ~50 μm and the diameter of nanowire ranges from 100 to 300 nm. The nanowires are uniformly distributed, well isolated, and parallel to each other. Fig. 1(c) shows the representative XRD patterns of the sample annealed at 400 °C. Two peaks emerge from the pattern of Ni–Pd/SiNWs at 44.12° and 51.66°. The former is the characteristic peak of Ni (111) with a slight shift and the peak at 51.66° is ascribed to the Pd (200) plane. The results confirm the Ni–Pd structure. The layer on the SiNWs is composed of Ni and Pd with Ni being the major constituent. The Ni coating is a dense layer containing Pd particles. The TEM image of the Pd–Ni/SiNWs provides further insight into the structure. As shown in Fig. 1(e), the Pd–Ni shell is well dispersed on the surface of the SiNWs and the thickness of this layer is about 10 nm. The selected area electron diffraction (SAED) patterns acquired from the Pd–Ni/SiNWs (inset in Fig. 1(e)) exhibit several well-defined rings, indicating that the Pd–Ni/SiNWs nanocomposites have a polycrystalline structure.

To evaluate the electrochemical activity, the Pd–Ni/Si and Pd–Ni/SiNWs are characterized by cyclic voltammetry (CV) in 1 M KOH in the potential range from −1 V to 0.6 V at a scanning rate of 50 mV s^{-1}. Fig. 2 shows the voltammograms obtained in the second cycle after reaching steady state. The activity of an electrode is decided not only by the catalytic properties but also surface area. The peaks between −0.95 V and −0.8 V (*versus* Ag–AgCl) are associated with hydrogen adsorption/desorption. The electrochemically active surface (EAS) of the Pd–Ni/SiNWs and Pd–Ni/Si electrodes is closely related to the surface area and can be measured by determining the Coulombic charge for the reduction of palladium oxide.[29] The Pd–Ni/SiNWs electrode has a larger EAS which is obviously greater than the geometric area. It leads to better dispersion of the catalysts, a larger interface on the Pd–Ni/SiNWs, and higher catalytic activity. There are two anodic peaks in the potential range between −0.6 V and 0.6 V (*versus* Ag–AgCl), one with a broad shoulder between −0.2 V and 0.3 V and the other one at 0.36 V with two reduction peaks at −0.48 V and 0.25 V. The voltammograms of the Pd–Ni/Si and Pd–Ni/SiNWs electrodes in 1 M KOH/1 M ethanol acquired at a scanning rate of 50 mV s^{-1} are shown in Fig. 3. Compared to the results obtained in the absence of ethanol, two oxidation peaks appear between −0.6 V and 0.2 V. In the forward scan, the oxidation peak (A) corresponds to oxidation of ethanol adsorbed on the catalysts. The re-oxidation peak (D) in the reverse scan is primarily associated with the removal of incompletinely oxidized carbonaceous species formed in the forward scan. During the process, the oxidation peak (B) current increases and potential moves towards the positive direction. At the same time, the reduction peak (C) current decreases continuously and the

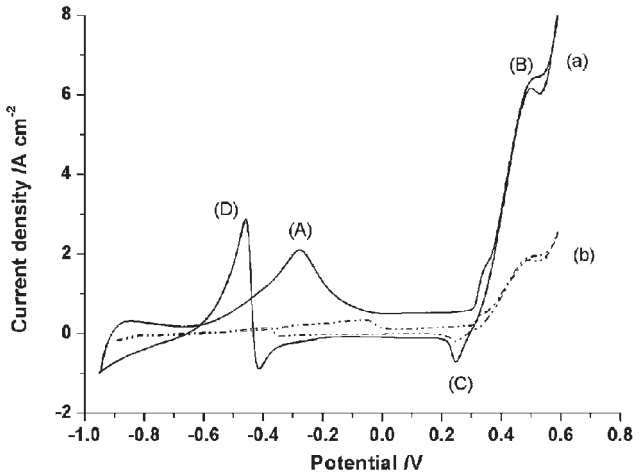

Fig. 3 Cyclic voltammograms of (a) Pd–Ni/SiNWs and (b) Pd–Ni/Si obtained in 1.0 M KOH with 1 M ethanol at room temperature at a scanning rate of 50 mV s^{-1}.

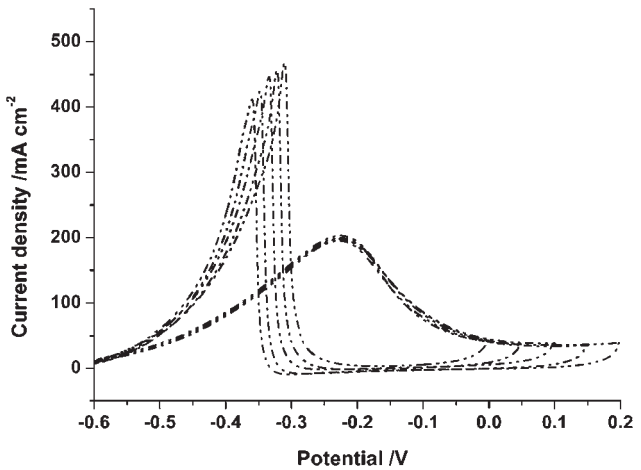

Fig. 4 Cyclic voltammograms of the Pd–Ni/SiNWs electrode on 1 M ethanol/1 M KOH for different upper scan limits at a scanning rate of 50 mV s^{-1}.

potential of the negative peak is not changed substantially with increased ethanol concentration. It is indicative of a simple redox reaction of nickel.

According to Fig. 3a and 3b, oxidation of ethanol is characterized by two oxidation peaks in the forward and reverse scans between −0.7 V and 0.2 V for both the Pd–Ni/Si and Pd–Ni/SiNWs electrodes. The current density measured from the Pd–Ni/SiNWs is clearly larger than that of the Pd–Ni/Si, and the onset potential (E_s), peak potential of the oxidation (E_p), and re-oxidation on Pd–Ni/SiNWs are 56 mV, 229 mV, and 80 mV, respectively. They are more negative than those determined from the Pd–Ni/Si electrode under the same conditions. It can be concluded that the Pd–Ni/SiNWs structure has a better catalytic activity than Pd–Ni/Si in ethanol oxidation and Pd–Ni/SiNWs can effectively reduce over-potentials and have better electrocatalytic activity. The Ni nanoparticles on the SiNWs exhibit a sensitive current response to ethanol but cannot oxidize ethanol. Based on the results shown in Fig. 2 and 3, the Pd–Ni/SiNWs

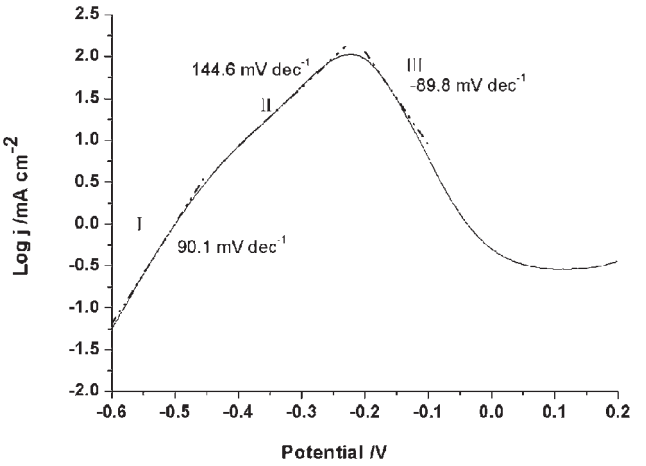

Fig. 5 Tafel plot of ethanol oxidation on the Pd–Ni/SiNWs electrode in 1 M KOH/1 M ethanol at 10 mV s^{-1}.

structure has a larger surface-to-volume ratio to better disperse the catalytic nanoparticles and the SiNWs backbone improves the catalytic properties as well.

Fig. 4 shows the CVs of the Pd–Ni/SiNWs electrode in 1 M ethanol/1 M KOH with different upper scan limits at a scanning rate of 50 mV s^{-1}. The lower limit is fixed at −0.6 V. The re-oxidation peak decreases and moves negatively whereas the oxidation peak in the anodic scan remains almost the same as the upper scan limit is increased. The results indicate that with a positive shift in the upper scan limit, ethanol oxidation becomes easier and the intermediate species can be effectively oxidized.

The activity of the Pd–Ni/SiNWs electrode is further assessed by obtaining the anodic Tafel polarization curves (*E versus* Log *j*) at a scanning rate of 10 mV s^{-1} in 1 M KOH + 1 M C_2H_5OH at 25 °C. The relationship between the potential and logarithmic current density is displayed in Fig. 5. There are three linear regions and the Tafel slopes of each region (I, II, and III) are 90.1 mV dec^{-1} 144.6 mV dec^{-1}, and −89.8 mV dec^{-1} in the potential range of −0.6 V to −0.45 V, −0.4 V to −0.23 V, and −0.2 V to −0.1 V, respectively. In the low potential range of −0.6 V to −0.45 V, the kinetics of ethanol oxidation is dominated by adsorption of hydroxyl groups on the Pd–Ni/SiNWs electrode. As the potential is increased, the Tafel slope increases from 90.1 to 144.6 mV dec^{-1} (Region II). The increase indicates that the kinetics of the ethanol oxidation reaction is affected by the formation of an oxide layer on the Pd–Ni/SiNWs surface at higher potentials. The Tafel slope reaches −89.8 mV dec^{-1} at higher potentials (Region III).

The current density curves at different temperatures from 25 °C to 80 °C in 1 M KOH solution/1 M ethanol acquired at the scanning rate of 50 mV s^{-1} are presented in Fig. 6. At 25 °C, the ethanol oxidation current peak and onset potential are −0.24 V and −0.62 V (*versus* Ag–AgCl), respectively. The current densities of the anodic oxidation peak and re-oxidation peak are improved as the temperature is increased. The maximum current density of the anodic oxidation peak is 210 mA cm^{-2} at 25 °C and it increases to 486 mA cm^{-2} at 60 °C. It may be due to the faster electrochemical kinetics of ethanol oxidation at a higher temperature. The re-oxidation peak shifts positively at the same time and the difference in the onset potentials becomes smaller.

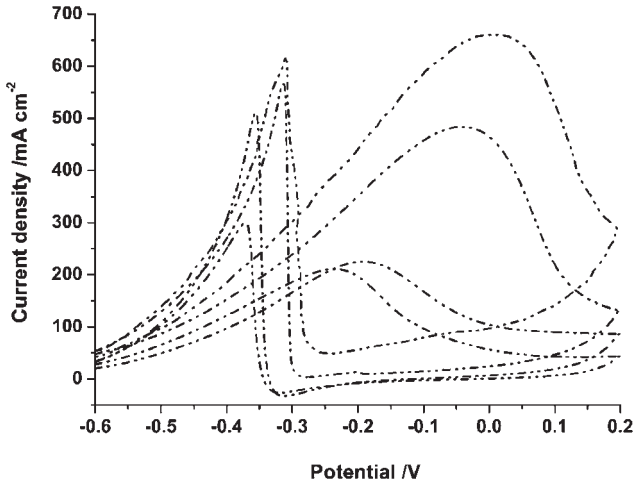

Fig. 6 Cyclic voltammograms of the Pd–Ni/SiNWs electrode in 1 M KOH/1 M ethanol at different temperatures at a scanning rate of 50 mV s^{-1}.

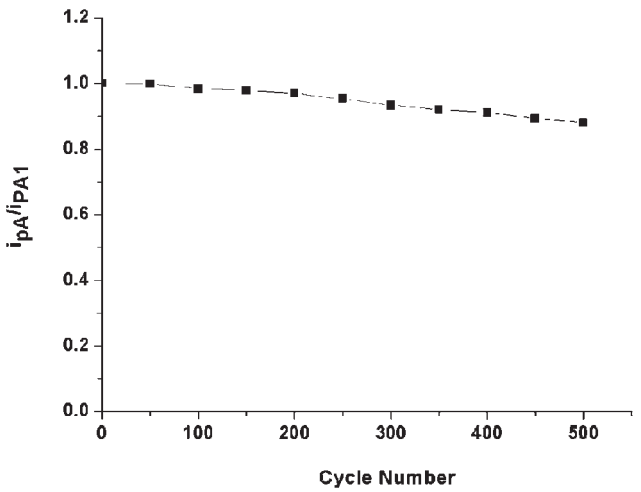

Fig. 7 Long-term stability of the Pd–Ni/SiNWs electrode in 1 M KOH solution/1 M ethanol at 50 mV s^{-1}.

The increase in the re-oxidation peak current at a higher temperature indicates that more intermediate species are produced. Hence, OH absorption on the Pd–Ni/SiNWs electrode diminishes, inducing the onset potential to shift negatively and the anodic oxidation to shift positively. Our data confirm that the temperature is a key parameter in ethanol oxidation.

The long-term stability of the electrode which is very important in practical applications is investigated in 1 M KOH solution/1 M ethanol. The relationship between i_{pA}/i_{PA1} (ratio between the current density of anodic oxidation peak A and current density of peak A in the first cycle) and time is depicted in Fig. 7. The i_{pA}/i_{PA1} ratios decrease gradually during successive scanning possibly due to accumulation of intermediate species on the catalyst surface or ethanol consumption. [30,31] Nevertheless, after 500 cycles, only 12% loss in the current density is observed from the Pd–Ni/SiNWs electrode. This can be confirmed further by the OCPT (open circuit potential time) measured under the same conditions as shown in Fig. 8. The

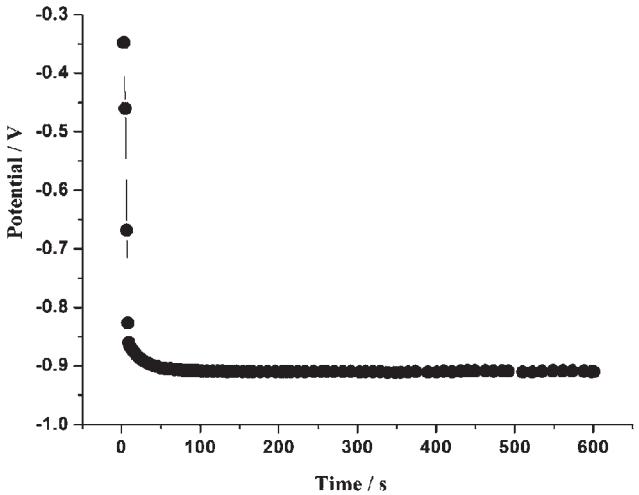

Fig. 8 OCPT curve of ethanol.

open circuit electromotive force is stable with time at −0.93 V. The results illustrate that the Pd–Ni/SiNWs electrode has reasonably good long-term stability which can be attributed to the stable film on the Pd–Ni nanoparticles.

From all results we can see that Pd–Ni is a good electrocatalyst for ethanol oxidation in alkaline media, and the SiNWs is an effective supporter for electrocatalyst. This is important to develop direct ethanol fuel cells. It could be attributed to three aspects:

Firstly, the Pd–Ni/SiNWs nanocomposite has excellent electrooxidation performance to ethanol, the activity of ethanol oxidation mainly due to the synergistic effect by the interaction among nickel, palladium and SiNWs.

Secondly, SiNWs as the backbone of electrocatalyst have a high volume to surface ratio and small curvature radii, not only increasing the reaction area but also promoting electron-transfer reactions, so accelerating the electrooxidation of ethanol.[32]

Thirdly, the microfabrication of SiNWs is compatible with IC processing techniques. The electrode annealed at 400 °C can form the NiSi layer between the Ni and SiNWs interface, which is resistant to OH^- etching and improves the electrocatalyst stability.[33]

4. Conclusion

A silicon-based structure with a large surface to volume ratio is demonstrated to effectively disperse catalytic nanoparticles. Electrochemical experiments indicate that Pd–Ni/SiNWs nanocomposites deliver good catalytic performance and long-term stability in ethanol oxidation. The direct ethanol fuel cells composed of this novel electrode are simple, inexpensive, and easily integrated into silicon-based devices.

Acknowledgements

This work was jointly supported by the Natural Science Foundation of Heilongjiang Province (No. F201008 and QC2011C092), Program for Young Teachers Scientific Research in Qiqihar University (Grant No. 2010k-Z02 and 2011k-Z01),

Excellent Young Scholars of Higher University of Heilongjiang Province No. 1251G067, Science and Technology Project of Qiqihar, Grant GYGG2010-03-1 and City University of Hong Kong Research Grant 9360110.

References

1 C.-G. Lee, M. Umeda and I. Uchida, *J. Power Sources*, 2006, **160**, 78.
2 K. Lee, J. Zhang, H. Wang and D. P. Wilkinson, *J. Appl. Electrochem.*, 2006, **36**, 507.
3 S. Rousseau, C. Coutanceau, C. Lamy and J. M. Léger, *J. Power Sources*, 2006, **158**, 18.
4 G. Andreadis, S. Q. Song and P. Tsiakaras, *J. Power Sources*, 2006, **157**, 657.
5 Z. B. Wang, G. P. Yin, J. Zhang, Y. C. Sun and P. F. Shi, *J. Power Sources*, 2006, **160**, 37.
6 S. Q. Song and P. Tsiakaras, *Appl. Catal., B*, 2006, **63**, 187.
7 F. Vigier, S. Rousseau, C. Coutanceau, J. M. Leger and C. Lamy, *Top. Catal.*, 2006, **40**, 111.
8 J. Ribeiro, D. M. dos Anjos, K. B. Kokoh, C. Coutanceau, J.-M. Léger, P. Olivi, A. R. deAndrade and G. Tremiliosi-Filho, *Electrochim. Acta*, 2007, **52**, 6997.
9 Z.-B. Wang, G.-P. Yin and Y.-G. Lin, *J. Power Sources*, 2007, **170**, 242.
10 Z. Liua, L. Huangb, L. Zhanga, H. Maa and Y. Dinga, *Electrochim. Acta*, 2009, **54**, 7286.
11 P. K. Shen and C. W. Xu, *Electrochem. Commun.*, 2006, **8**, 184.
12 D. Basu and S. Basu, *Electrochim. Acta*, 2011, **56**, 6106.
13 B. R. Tao, J. Zhang, S. C. Hui and L. J. Wan, *Sens. Actuators, B*, 2009, **142**, 298.
14 M. C. Pham, F. Adami, P. C. Lacaze, J. P. Boucet and J. E. Dubois, *J. Electroanal. Chem.*, 1986, **201**, 413.
15 C. Fan, D. L. Piron, A. Sleb and P. Paradis, *J. Electrochem. Soc.*, 1994, **141**, 382.
16 P. V. Samant, J. B. Fernandes, C. M. Rangel and J. L. Figueiredo, *Catal. Today*, 2005, **173**, 102.
17 F. Hu, F. Ding, S. Song and P. K. Shen, *J. Power Sources*, 2006, **163**, 415.
18 H. L. Pang, J. P. Lu, J. H. Chen, C. T. Huang, B. Liu and X. H. Zhang, *Electrochim. Acta*, 2009, **54**, 2610.
19 D. Yuan, C. Xu, Y. Liu, S. Tan, X. Wang and Z. Wei, *et al.*, *Electrochem. Commun.*, 2007, **9**, 2473.
20 M. W. Xu, G. Y. Gao, W. J. Zhou, K. F. Zhang and H. L. Li, *J. Power Sources*, 2008, **175**, 217.
21 C. Xu, P. K. Shen and Y. Liu, *J. Power Sources*, 2007, **164**, 527.
22 H. Wang, C. Xu, F. Cheng and S. P. Jiang, *Electrochem. Commun.*, 2007, **9**, 1212.
23 R. Ryoo, S. Joo, H. Kruk and M. Jaroniec, *Adv. Mater.*, 2001, **13**, 677.
24 J. S. Lee, S. H. Joo and R. Ryoo, *J. Am. Chem. Soc.*, 2002, **124**, 1156.
25 M. Kruk, M. Jaroniec, T. W. Kim and R. Ryoo, *Chem. Mater.*, 2003, **15**, 2815.
26 F. J. Miao, B. R. Tao, L. Sun, T. Liu, J. C. You, L. W. Wang and P. K. Chu, *Sens. Actuators, A*, 2010, **160**, 48.
27 J. Shi, P. L. Ci, F. Wang, H. Peng, P. X. Yang and L. W. Wang, *Electrochim. Acta*, 2011, **56**, 4197.
28 M. Bhaskaran, S. Sriram and L. W. Sim, *J. Micromech. Microeng.*, 2008, **18**, 095002.
29 C. W. Xu and P. K. Shen, *Chem. Commun.*, 2004, 2238.
30 J. Kua and W. A. Goddard III, *J. Am. Chem. Soc.*, 1999, **121**, 10928.
31 Z. B. He, J. H. Chen, D. Y. Liu, H. Tang, W. Deng and Y. F. Kuang, *Mater. Chem. Phys.*, 2004, **85**, 396.
32 J. O. Howell and R. M. Wightman, *Anal. Chem.*, 1984, **56**, 524.
33 M. Bhaskaran, S. Sriram and L. W. Sim, *J. Micromech. Microeng.*, 2008, **18**, 095002.